IEEE Photonics Journal
An IEEE Photonics Society Publication

Open Access

Electro-Optic Plasmonic Modulator With Direct Coupling to Silicon Waveguides

Volume 9, Number 6, December 2017

Abd Al Rahman Mohamed
Lamees A. Shahada
Mohamed A. Swillam

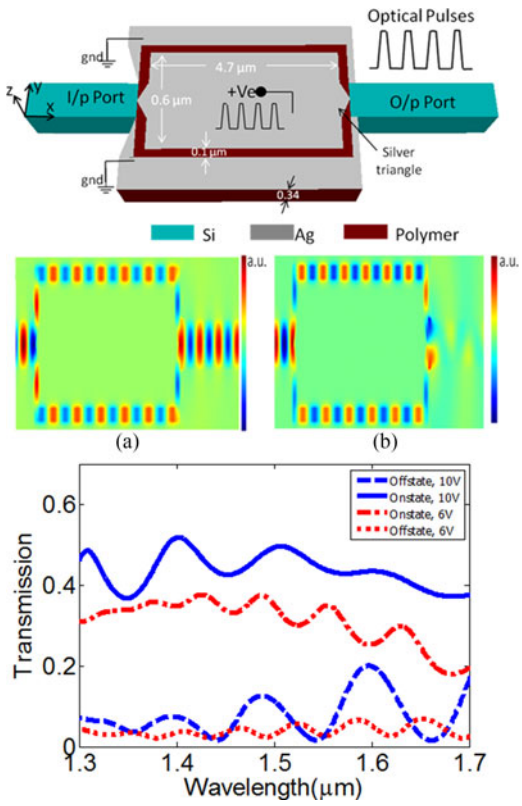

DOI: 10.1109/JPHOT.2017.2757014
1943-0655 © 2017 IEEE

IEEE photonics SOCIETY

IEEE

Electro-Optic Plasmonic Modulator With Direct Coupling to Silicon Waveguides

Abd Al Rahman Mohamed,[1] Lamees A. Shahada,[2] and Mohamed A. Swillam [1]

[1]Department of Physics, School of Sciences and Engineering, The American University in Cairo, New Cairo 11835, Egypt
[2]Department of Chemistry and Earth Sciences, College of Arts and Science, Qatar University, Doha 2713, Qatar

DOI:10.1109/JPHOT.2017.2757014

Manuscript received September 5, 2017; revised September 16, 2017; accepted September 21, 2017. Date of current version November 3, 2017. This work was supported by the NPRP Award (NPRP7-456-1-085) from the Qatar National Research Fund (member of the Qatar Foundation). Corresponding author: Mohamed A. Swillam (e-mail: m.swillam@aucegypt.edu).

Abstract: A novel plasmonic Mach–Zehnder interferometer is proposed with a nonlinear polymer. Orthogonal junction coupling between silicon and plasmonic waveguides is exploited to omit the need for tapers, and in turn, reduce the footprint. An extinction ratio of about 16 dB is produced at a voltage-length product of 47 V μm. An insertion loss of 3.38 dB is achieved including the coupling to and from the silicon access waveguide. The orthogonal coupling provides wideband operation, high efficiency, low loss, and compact size for our design.

Index Terms: Integrated optics devices, modulators, electro-optical devices, surface plasmons.

1. Introduction

Electrical interconnects limit the processors computational power, due to the RC delay in communication within the cores of the processor and between different cores. Optical Interconnects that have the privilege of working at much higher speeds offers a good solution for such problem [1], [2]. A key component in any on chip optical system is the electro-optic modulator. High compactness, low Power consumption, large extinction ratio, and high speed are the most desirable properties of the electro-optic modulator.

Silicon photonics technology has attracted considerable attention in the last decade due to its ability to fabricate low loss waveguide based components. Modulation, in general, occurs through utilizing nonlinear effect, or through utilizing index change induced due to free carrier injection [3]–[6]. However, silicon photonic devices miniaturizing in the nano-scale is not easy due to the diffraction limit.

Plasmonics, on the other hand, has the unique ability of confining light in metal-dielectric interfaces in the nano scale. Hence, it can increase the light-mater interaction and allow for shorter devices compared to silicon photonics [7]. On the other hand, plasmonics suffer from high propagation losses and should be compact in size to alleviate this drawback. A hybrid technology that exploits the low path losses advantage of silicon photonics and the tight light confinement of plasmonic devices can be an attractive platform specially for on chip modulators [6], [8], such a hybrid

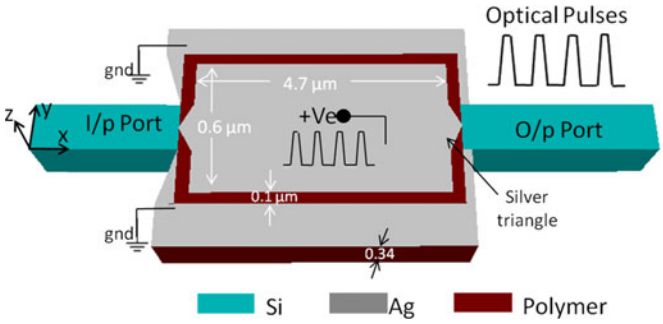

Fig. 1. The MZM, with input and output silicon waveguides, the modulator arms are plasmonic slot waveguides filled with nonlinear polymer, with two silver triangles at the input and output. The x-y plane contains the top plane of the modulator.

platform is known as the hybrid plasmonic platform. Plasmonic crystal nano-cavities [9*], hybrid photonic-plasmonic resonator [10*], optical trapping device [11*] and a biosensing application [12*] have been demonstrated as applications from the hybrid photonic plasmonic systems.

Plasmonic modulators, can be built using various configurations including resonance topology, electro-absorption, and interference mechanism. Plasmonic resonators have a relatively small footprint, and low power consumption [13]. However, they suffer from high sensitivity to temperature and process variations, requiring them stabilization circuitry, and in turns more power and area consumption [14]. On the other hand, Mach-Zehnder doesn't suffer from temperature and process variations, as these variations usually cancel out in the symmetric arms of the Mach-Zehnder [15]. Electro-absorption modulator, on the other hand, dissipates more heat than the other modulators [16], [17]. Graphene and Indium Tin oxide (ITO) are widely used for such applications [18]–[22]. Lastly, interferometer modulators including Mach-Zehnder modulators (MZM) for example, are low power consumers, but they lack the small footprint advantage of their competitors and hence higher insertion losses are expected [22]–[24].

In this paper, we utilize the advantages of both the plasmonic organic MZM and the orthogonal junction coupler presented in [25], [26]. These two platforms together are able to make a good compromise between modulator length, footprint, extinction ratio, insertion loss, and energy consumption relative to the previous works, as will be shown latter. The orthogonal junction enables direct coupling between silicon interconnects used in routing data, and plasmonic waveguides of the MZM, without the need for a tapering or any special junction, this advantage is the main source of enhancement in our design.

In the next section, we present the working principle of the modulator. The third section presents the design methodology and optimization process of the modulator. The fourth section presents the results accompanied by a discussion of the work significance.

2. Operation Principle

The MZM device consists of input silicon waveguide, coupled to a plasmonic slot orthogonal junction, that is connected to the plasmonic slot arms of the MZM. Lastly the MZM arms are coupled to the output silicon waveguide again through an orthogonal coupler, as shown in Fig. 1. The waveguides are optimized such that lateral momentum component of the silicon waveguide mode matches the momentum of the plasmonic slot waveguide (PSW) to ensure maximum coupling between the two waveguides. This approach has theoretically and experimentally been verified to provide efficient, wide band, non-resonant coupling from/to silicon waveguides to/from PSWs [25], [26].

The plasmonic waveguide core is filled with a nonlinear electro-optic polymer (EOP) that exhibits the Pockels effect. If no voltage is applied, the light propagates to the combiner, where the fields interfere constructively, Fig. 2(a). Once the voltage is applied, the refractive indices of the upper and lower paths differ, so the light propagate in each arm at different speed. The length of the

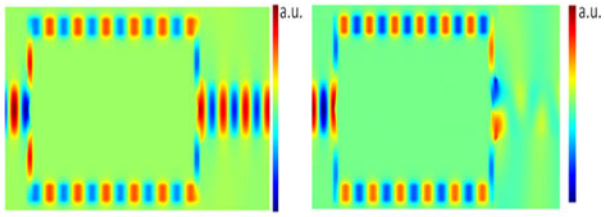

Fig. 2. The z-component of the magnetic field (Hz) at wavelength equals to 1.55 μm for the On state of the modulator (a), and the Off state (b).

plasmonic waveguide is designed to induce sufficient phase difference between the two paths to create a destructive interference at the combiner as shown in Fig. 2(b).

Positive voltage is applied on the middle silver island, and a ground is applied on the exterior silver islands as shown in Fig. 1. Accordingly, the electric field direction is outward from the middle metal island. The PSWs along the y-axis located at the splitter and the combiner, have an electric field direction in the negative and positive x-direction respectively. This biasing method is called the push-pull configuration. Only the plasmonic waveguide parts along the x-axis in each arm will have a different field direction, in turns, they will be the only contributors in creating the phase difference accumulation.

It is worth noting that the Silicon-PSW orthogonal junction designed in [25], [26] were optimized, where the slot was air filled. Now the slot is filled with the EOP which increases the momentum of the plasmonic mode inside the slot. This required a modification of the original design to allow for better matching, efficient splitting, and minimize the reflection to the main waveguide. Accordingly, the design has been optimized with two major modifications. The first one, is the addition of silver triangles to the middle metal island at the splitter and combiner. The silver triangles help in guiding the power in the splitter and out of the combiner. Also, they decrease the reflections from the orthogonal junction combiner which cause an undesired cavity effect for the proper work of the MZM. The base side of the isosceles silver triangle is equal to the width of the silicon waveguide. The second modification is using a 100 nm flat metal surface instead of the tapered one at the combiner, as shown in Fig. 1, this is found more capable of distributing the power at the output of the silicon waveguide, such that the fields interfere destructively in a more efficient way, which enhances the extinction ratio.

3. Our Novel Designs

A full electromagnetic analysis based on the finite-difference time-domain method is utilized to verify the design concept and optimize the design using [27]. The smallest mesh size is 10 nm. 2D simulations were used as a preliminary step for 3D simulations. Throughout 2D simulations, the Si on SiO2 waveguide were modeled using the effective index method. In 3D simulations, the refractive index of Si and SiO2 were chosen to be 3.45 and 1.45 respectively. The Johnson-Christy material model is used for silver [28], which is an experimentally verified model. The effect of the angle of the wedge with the silicon waveguide at the input side is minor as long as it is between 45 degrees and 80 degrees. The polymer used is Dispersive Red 1-poly-methyl-methacrylate (DRI-MMA) side chain copolymer [30]. The electro-optic side chain copolymers are known to be stable and can be used in long term photonic devices [30]. The thickness of the polymer layer is the same as surrounding silver.

Fig. 3 shows the transmission of the modulator Vs Si waveguide width, at a slot gab size of 100 nm, with arbitrary arm lengths, the 400 nm is chosen for maximum coupling. The height of the silicon waveguide was chosen to be 340 nm to match a typical sold silicon on insulator (SOI) wafer. The refractive index change of the polymer by Pockels effect follows (1) [29].

$$n = n_0 \pm \frac{1}{2} \times r_{33} \times {n_0}^3 E \tag{1}$$

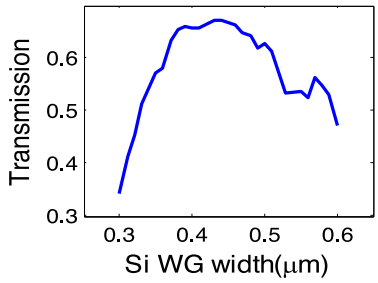

Fig. 3. The transmission (output power/input power) of the modulator versus the width of the silicon waveguide (Si WG) at a height equal to 340 nm, and wavelength equal to 1.55 μm at zero voltage (On state).

TABLE 1
Refractive Index of Polymer and Effective Index of the Plasmonic WG Arms Under 10 V

	Arm(1)	Arm(2)	Δn
Refractive index	1.6614	1.5386	0.1228
Effective index	2.2464	2.0667	0.1797

Where n_0 is the refractive index of the polymer at no voltage, it is equal to 1.6, r33 is the electro-optic coefficient of first order nonlinearity of the polymer, it is equal to 300 pm/V [30], and E is the electric field across the polymer. The electric field is V/g, where V is the voltage difference across any of the two arms of the Mach-Zehnder, g is the slot width of the plasmonic waveguide. The sign in (1) can be positive or negative according to the direction of the applied electric field. We chose g to be 0.1 μm to be convenient for future fabrication. The device is feasible to be fabricated using electron beam lithography similar to the design in [24].

By applying 10 V on the middle silver area, the refractive indices of the polymer of each arm are calculated using (1), and the effective indices of the plasmonic waveguides are calculated using modal analysis [27]. Both refractive and effective indices are shown in Table 1. The large variation in the effective index is an evidence on the high light-matter interaction and confinement.

The phase delay is related to the propagation constant through $\Delta\beta L = \emptyset$, where L is the Mach-Zehnder arm length, $\emptyset$ is the phase difference on the ends of each arm, and β is the propagation constant of the plasmonic mode. The length of the modulator is as given by (2).

$$L = \frac{\pi}{\Delta\beta} = \frac{\lambda}{2\Delta n_{eff}} \tag{2}$$

The length is calculated to be 4.33 μm. Through 3D simulations, on applying 10 V, the optimum value for the length of the arms, at which the modulator has minimum transmission, was found to be 4.7 μm. Consequently the length of the plasmonic waveguide along the x direction is 4.7 μm and the sides along the y direction were chosen to be 0.6 μm, which is lower than previous published work as will be shown latter. The main performance enhancer is the addition of the orthogonal coupling junctions which is shorter than the tapper junctions used before [24].

4. Modulator Characteristics

To be able to quantify the performance of an optical modulator, few important measures should be calculated. The main parameters are the extinction ratio, insertion loss, dimensions, bandwidth,

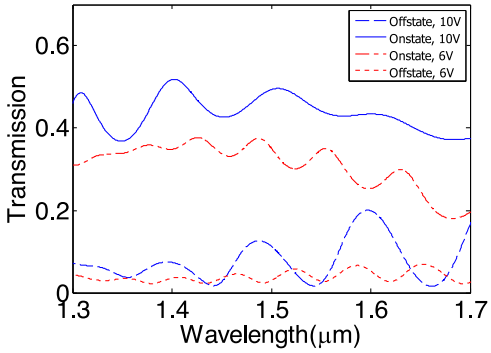

Fig. 4. The transmission (output power/input power) in the On and Off states. The blue solid is for the 10 V modulator whose length is 4.7 μm. The red dashed is for the 6 V modulator whose length is 8.1 μm.

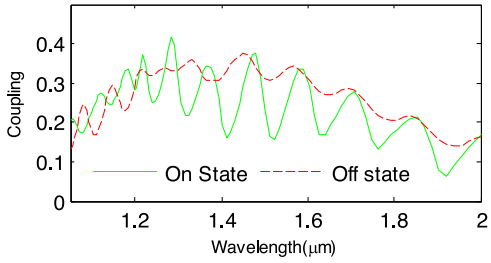

Fig. 5. The two curves show the normalized coupling in any of the two arm, in the on (solid green) and off (dashed red) states. Both are for the 10 V modulator (the legend is for both graphs).

energy per bit, and the reflections. Each of these parameters are defined, compared and discussed with the state of the art values in the following subsections.

The main output of our analysis - from which we will discuss most of the modulator metrics - is the transmission (output power/input power) of the modulator, shown in Fig. 4. The transmission curve was calculated from 3D simulations for two cases. The first at biasing voltage equal to 10 V, and the second for biasing voltage equal to 6V. The main parameters of the modulator is extracted in Table 2 for the 1.55 μm wavelength. The parameters for state of the art designs in literature are added to the same table. The designs presented in the table are: [23], [25] which are plasmonic MZM with tapered couplers of different configurations, and [20] which is an electro-absorption modulator.

Extinction ratio is a key parameter in modulators, it quantifies the strength of modulation by measuring the difference between the output power in the on and off states. 3D simulations were done to get accurate values for extinction ratio at 10 V and 6 V biasing. An extinction ratio of 15.8 dB is calculated at 10 V, and approximately 11 dB is calculated at 6 V, both at 1.55 μm.

To show the superiority of this performance, we compared our results to state of the art MZM. Our device has higher extinction ratio than the 6dB presented in [24] and the 7.3 dB presented in [23], as shown below in Table 2. Both designs presented in [23], [24] use different configurations of tapered couplers; that shows the effectiveness of using orthogonal coupling. Also we compared our work to a state of art electro-absorption modulator presented [20], and our device also shows higher extinction ratio as shown in Table 2 below.

Insertion loss is a critical measure for the optical losses in the device. Higher losses in any of the devices in an interconnect system, means more energy consumption in the whole processor; energy consumption is a critical issue in processors. The optical losses include the coupling and waveguide and material losses. Our device shows 3.38 dB and 4.6 dB at 10 V and 6 V biases, respectively. This performance is a step ahead the previously published work in plasmonic MZM as shown in Table 2 below.

TABLE 2
Comparison Between Plasmonic Modulators

Comparison Parameters	Our Work at 10V	Our Work at 6V	C.Haffner (2015) [24]	Shiyang Zhu (2010) [16]	Volker J. Sorger(2012) [20]
Extinction Ratio	15.8 dB	11 dB	6 dB	7.3 dB	5 dB
Insertion Loss	3.38 dB	4.6 dB	5 dB	8 dB	1 dB
Energy Consumption	40.82 fJ bit-1	25.5 fJ bit-1	25 fJ bit-1	–	56 fJ bit-1
Voltage	10 V	6 V	6 V	5.6 V	4 V
Length	4.7 μm	8.1 μm	10 μm	3.7 μm	5 μm

A main target of our work is to enhance the size of the MZM. the main parameter that quantify the size of a MZM is the voltage length product. Our device shows 47 Vμm voltage length product, which is 21.5% lower than the state of the art plasmonic MZM presented in [24].

Optical bandwidth can be quantified from the transmission response in Fig. 4, the 6 V biased modulator, shows a wide band operation specially for the region starting from 1.3 μm till 1.55 μm. The 10 V biased modulator shows a narrow band response, due to the ripples in the response. These ripples in the transmission response is due to a resonating wave that bounces between the two orthogonal junctions. This resonance effect is more evident in the 10 V modulator because it has a shorter length, in turns lower losses and higher quality factor. Electrical bandwidth determines the maximum bit rate of the modulator. Since our device is smaller than the one reported in [24] and the same electro-optic material is used, then it is estimated to have at least the same bit rate that exceeded 54 Gbit/s.

The energy per bit consumption for the modulators in optical interconnects should be as low as 50 fJ bit-1 [31]. We estimated the energy consumption using a capacitance model, the capacitance is calculated analytically. Our modulator is below this limit at both the 10 V and 6 V biased modulators. In comparison to the modulators presented in Table 2, our 6 V biased modulator shows similar energy per bit value to [24], and both our devices show lower values than the electro-absorption modulator presented in [20]. Resonators show lower energy consumption, but as mentioned before, resonators are much less stable against process and temperature variations [14], [15].

Lastly, the coupling losses in both modulator arms ranges between 1.87 dB to 0.97 dB in the range of wavelength between 1.4 μm to 1.6 μm, in the on state of the 10 V biased modulator as shown in Fig 5. In the off state, the coupling decreases due to the effective index contrast between the silicon and plasmonic waveguides.

5. Conclusion

An organic plasmonic Mach-Zehnder modulator was presented. We took advantage of the orthogonal junction coupling technique. The footprint of the modulator is decreased to 0.6 μm $\times$ 4.7 μm by the omission of the tapering sections used before [24] to couple in and out of plasmonic waveguides. Extinction ratio of 15.8 dB and insertion loss of 3.38 dB at 10 volts was achieved in the 3D simulations. The voltage length product for the modulator is 47 V μm. The orthogonal junction coupler enhances the extinction ratio and insertion loss of the organic Mach-Zehnder plasmonic modulator, while keeping the voltage length product approximately the same.

Acknowledgment

This report was made possible by a NPRP award [NPRP 7-456-1-085] from the Qatar National Research Fund (a member of The Qatar Foundation). The statements made herein are solely the responsibility of the authors.

References

[1] Semiconductor Industry Association, The International Technology Roadmap for Semiconductors, 2013. [Online]. Available: http://www.itrs2.net/2013-itrs.html
[2] Semiconductor Industry Association, The International Technology Roadmap for Semiconductors, 2015. [Online]. Available: http://www.itrs2.net/2013-itrs.html
[3] D. Korn *et al.*, "Silicon-organic hybrid (SOH) IQ modulator using the linear electro-optic effect for transmitting 16QAM at 112 Gbit/s," *Opt. Exp.*, vol. 21, pp. 13219–13227, 2013.
[4] H. Xu *et al.*, "High-speed silicon modulator with band equalization," *Opt. Lett.*, vol. 39, pp. 4839–4842, 2014.
[5] A. Dhiman, "Silicon photonics: A review," *IOSR J. Appl. Phys.*, vol. 3, pp. 67–79, 2013.
[6] G. T. Reed, G. Mashanovich, F. Y. Gardes, and D. J. Thomson, "Silicon optical modulators," *Nature Photon.*, vol. 4, pp. 518–526, 2010.
[7] D. K. Gramotnev and S. I. Bozhevolnyi, "Plasmonics beyond the diffraction limit," *Nature Photon.*, vol. 4, pp. 83–91, 2010.
[8] Z. Ma, Z. Li, K. Liu, C. Ye, and V. J. Sorger, "Indium-tin-oxide for high-performance electro-optic modulation," *Nanophotonics*, vol. 4, pp. 198–213, 2015.
[9] X. Yang *et al.*, "Hybrid photonic−Plasmonic crystal nanocavities," *ACS Nano*, vol. 5, pp. 2831–2838, 2011.
[10] Y.-F. Xiao *et al.*, "Strongly enhanced light-matter interaction in a hybrid photonic-plasmonic resonator," *Phys. Rev. A*, vol. 85, 2012, Art. no. 031805.
[11] C. Ciminelli, D. Conteduca, F. Dell'Olio, and M. N. Armenise, "Design of an optical trapping device based on an ultra-high Q/V resonant structure," *IEEE Photon. J.*, vol. 6, no. 6, Dec. 2014, Art. no. 0600916.
[12] D. Conteduca *et al.*, "Rigorous design of an ultra-high Q/V photonic/plasmonic cavity to be used in biosensing applications," *Opt. Laser Technol.*, vol. 77, pp. 151–161, 2016.
[13] A. O. Zaki, N. H. Fouad, D. C. Zografopoulos, R. Beccherelli, and M. A. Swillam, "Low-power compact hybrid plasmonic double-microring electro-optical modulator," *Proc. SPIE*, vol. 9744, 2016, Art. no. 97441K.
[14] C. Sun *et al.*, "Single-chip microprocessor that communicates directly using light," *Nature*, vol. 528, pp. 534–538, 2015.
[15] B. Guha, A. Gondarenko, and M. Lipson, "Minimizing temperature sensitivity of silicon Mach-Zehnder interferometers," *Opt. Exp.*, vol. 18, pp. 1879–1887, 2010.
[16] S. Zhu, G. Q. Lo, and D. L. Kwong, "Electro-absorption modulation in horizontal metal-insulator-silicon-insulator-metal nanoplasmonic slot waveguides," *Appl. Phys. Lett.*, vol. 99, 2011, Art. no. 151114.
[17] A. O. Zaki, K. Kirah, and M.A. Swillam, "Hybrid plasmonic electro-optical modulator," *Appl. Phys. A*, vol. 122, pp. 473–479, 2016.
[18] M. Liu *et al.*, "A graphene-based broadband optical modulator," *Nature*, vol. 474, pp. 64–67, 2011.
[19] J.-S. Shin and J. T. Kim, "Broadband silicon optical modulator using a graphene-integrated hybrid plasmonic waveguide," *Nanotechnology*, vol. 26, 2015, Art. no. 365201.
[20] V. J. Sorger, N. D. Lanzillotti-Kimura, R.-M. Ma, and X. Zhang, "Ultra-compact silicon nanophotonic modulator with broadband response," *Nanophotonics*, vol. 1, pp. 17–22, 2012.
[21] V. E. Babicheva, "Ultra-compact plasmonic waveguide modulators," DTU FOTONIK, Dept. Photon. Eng., Tech. Univ. Denmark, Kongens Lyngby, Denmark, 2013.
[22] M. Xu *et al.*, "Design of an electro-optic modulator based on a silicon-plasmonic hybrid phase shifter," *J. Lightw. Technol.*, vol. 31, no. 8, pp. 1170–1177, Apr. 2013.
[23] K. F. MacDonald and N. I. Zheludev, "Theoretical investigation of silicon MOS-type plasmonic slot waveguide based MZI modulators," *Laser Photon. Rev.*, vol. 4, pp. 562–567, 2010.
[24] C. Haffner *et al.*, "All-plasmonic Mach–Zehnder modulator enabling optical high-speed communication at the microscale," *Nature Photon.*, vol. 9, pp. 525–528, 2015.
[25] C. Lin, H. M. Wong, B. Lau, M. A. Swillam, and A. S. Helmy, "Efficient broadband energy transfer via momentum matching at hybrid junctions of guided-waves," *Appl. Phys. Lett.*, vol. 101, 2012, Art. no. 123115.
[26] B. Lau, M. A. Swillam, and A. S. Helmy, "Hybrid orthogonal junctions: Wideband plasmonic slot-silicon waveguide couplers," *Opt. Exp.*, vol. 18, pp. 27048–27059, 2010.
[27] Lumerical Solutions, Inc., Vancouver, BC, Canada. 2003. [Online]. Available: http://www.lumerical.com/tcad-products/fdtd/
[28] P. B. Johnson and R. W. Christy, "Optical constants of noble metal," *Phys. Rev. B*, vol. 6, no. 12, pp. 4370–4379, 1973
[29] A. J. Iverson *et al.*, "Electro-optic Pockels cell voltage sensors for accelerator diagnostics," College Eng., Montana State Univ., Bozeman, MT, Canada, 2004.
[30] S. Michel, J. Zyss, I. Ledoux-Rak, and C. T. Nguyen, "High-performance electro-optic modulators realized with a commercial side-chain DR1-PMMA electro-optic copolymer," in *Proc. SPIE, Int. Soc. Opt. Photon.*, 2010, Art. no. 75990I.
[31] D. A. B. Miller, "Device requirements for optical interconnects to silicon chips," *Proc. IEEE*, vol. 97, no. 7, pp. 1166–1185, Jul. 2009.